

Resonant X-Ray Magnetic Scattering from CoO

Jun-ichi IGARASHI and Manabu TAKAHASHI

Faculty of Engineering, Gunma University, Kiryu, Gunma 376-8515

(Received)

We analyze the recent experiment [W. Neubeck *et al.*, Phys. Rev. B **60** (1999) R9912] for the resonant x-ray magnetic scattering (RXMS) around the K edge of Co in the antiferromagnet CoO. We propose a mechanism of the RXMS to make the $4p$ states couple to the magnetic order: the intraatomic exchange interaction between the $4p$ and the $3d$ states and the p - d mixing to the $3d$ states of neighboring Co atoms. These couplings induce the orbital moment in the $4p$ states and make the scattering tensor antisymmetric. Using a cluster model, we demonstrate that this modification gives rise to a large RXMS intensity in the dipole process, in good agreement with the experiment. We also find that the pre-edge peak is generated by the transition to the $3d$ states in the quadrupole process, with negligible contribution of the dipole process. We also discuss the azimuthal angle dependence of the intensity.

KEYWORDS: resonant x-ray scattering, magnetic scattering, K -edge, CoO, quadrupole transition

§1. Introduction

Resonant x-ray scattering has recently attracted much interest as a useful tool to investigate the magnetic order. The resonant enhancement for magnetic Bragg reflections has been observed in transition metals¹⁾ and their compounds.^{2,3,4)} For the resonant enhancement to be observable on the magnetic Bragg spots, orbitals have to couple with the magnetic order. It is usually achieved through the spin-orbit interaction. In this paper, we study the mechanism of the resonant x-ray magnetic scattering (RXMS) by focusing our attention on a typical material, CoO, where orbitals are strongly coupled to the magnetic order, and analyze the recent RXMS experiment by Neubeck *et al.*³⁾

In CoO, Co atoms form an fcc lattice with a small tetragonal distortion of $c/a < 1$ below the Néel temperature $T_N = 292$ K. It is a type II antiferromagnet (AF) characterized by a wavevector \mathbf{Q} , which is directed to one of four body-diagonals in the fcc lattice, thus forming K domains.^{5,6)} Although a non-collinear magnetic order has been proposed so far,^{7,8)} it is quite reasonable to assume a collinear magnetic order in the analysis of the RXMS intensity, since the RXMS signal is separately observed for different domains in the experiment.³⁾ The spin vector lies in the plane

perpendicular to the AF modulation direction; three directions are possible, forming S domains.⁶⁾ For an example, the spins are directed to $(-1, -1, 2)$, $(-1, 2, -1)$, or $(2, -1, -1)$, which we call domains S_1 , S_2 , and S_3 , in the K domain with $\mathbf{Q} = (\frac{1}{2}, \frac{1}{2}, \frac{1}{2})$. Figure 1 depicts schematically this domain. In total, we have 12 domains. The orbital moment is known to be as large as $\sim 1\mu_B$.⁵⁾ This material was expensively studied for decades ago by Kanamori,⁹⁾ who pointed out that the large orbital moment causes a large magnetostriction.

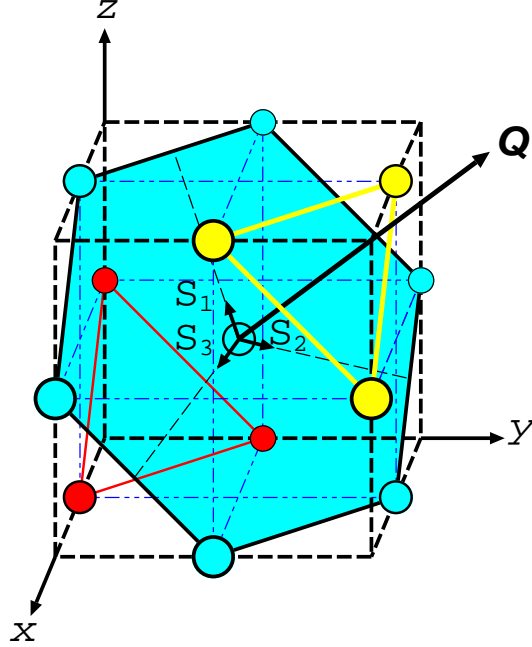


Fig. 1. Sketch of a CoO crystal (only Co atoms are shown). Wave vector $\mathbf{Q} = (\frac{1}{2}, \frac{1}{2}, \frac{1}{2})$ characterizes an antiferromagnetic modulation direction. Three arrows in a plane perpendicular to \mathbf{Q} indicate possible spin directions. Spins of solid, gray, and open circles align alternately.

For photons with energy near the K edge, the $4p$ states become occupied in the intermediate states of the dipole process. The $4p$ states, different from the $3d$ states, are highly extended in space. To have a feeling of the character of the wavefunctions, we show in Fig. 2 the radial wave functions calculated within the Hartree-Fock approximation¹⁰⁾ for a free Co^{2+} atom. The concept of localized orbitals loses its clear meaning outside the ion radius in solids. Since the $4p$ states have large weights outside the ion radius, treating them as local orbitals in a cluster model may limit the usefulness of the model to a qualitative level. Nevertheless, we use a cluster model to make clear the mechanism of the RXMS in CoO. We hope this will serve as a first step to more quantitative study based on band structure calculations.

A closely related phenomenon where the $4p$ states are involved is the resonant x-ray scattering for the orbital order in LaMnO_3 .^{11,12)} This case has been thoroughly studied with treating the $4p$ states of Mn as a band.^{13,14,15)} It has been shown that the $4p$ states of Mn is mainly modified by the Jahn-Teller distortion via the oxygen potential on the neighboring sites, and that this modification gives rise to non-vanishing diagonal elements in the scattering tensor, leading to a large main peak. On the other hand, the mechanism of the RXMS for CoO is much complicated. The $4p$ states are required to couple to the magnetic order. This is achieved through the coupling to the $3d$ states which constitute the magnetic order. Two processes are likely to be effective to make the $4p$ states couple to the $3d$ states: the intraatomic exchange interaction and the p - d mixing to the $3d$ states of neighboring Co atoms. We demonstrate that these couplings give rise to a modification of the $4p$ states and make the scattering tensor antisymmetric. The RXMS intensity thus generated seems much smaller than the intensity generated by the Jahn-Teller effect in LaMnO_3 , but is sufficiently larger than the pre-edge intensity coming from the quadrupole process. Note that the $3d$ states having orbital moment is crucial to generate the RXMS intensity. The amplitude of exciting an electron with up spin (up spin process) is generally different from that of the exciting an electron with down spin (down spin process). However, the sum of the amplitudes for the up and down spin processes become the same at each site if the system has no orbital moment; the RXMS intensity is not generated by such spin scattering processes alone, since the total amplitude is given by the difference between those at the A and B sublattices.

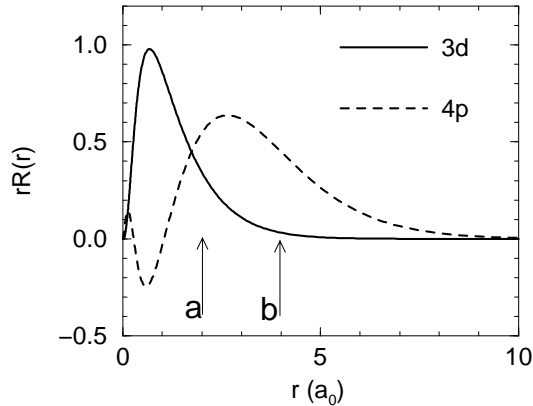


Fig. 2. Radial wave functions (multiplied by the radius) in the $3d^7$ configuration of a free Co^{2+} atom. The radius r is measured in units of the Bohr radius a_0 . The arrow a indicates the ion radius, which is defined by the half of the distance between the Co and O atoms in the CoO crystal. The arrow b indicates the distance to a neighboring O atom.

In addition to the dipole process, we also consider the quadrupole process, which gives rise to a

pre-edge peak. Although the dipole process can also contribute to the pre-edge peak through the p -symmetric states mixing to the $3d$ states of neighboring Co atoms, this contribution is found to be much smaller than that of the quadrupole process. This result is consistent with the experiment.³⁾ Note that, for the pre-edge peak in LaMnO_3 , the contribution from the dipole process is predicted to be much larger than that of the quadrupole process.¹⁶⁾

This paper is organized as follows. In § 2, we formulate the RXMS intensity. In § 3, we present a cluster model and discuss the relevant $4p$ and $3d$ states. In § 4, we show the calculated results for the RXMS intensity in comparison with the experiment. Section 5 is devoted to concluding remarks. In the Appendix, the geometrical factor is explicitly given for the dipole and quadrupole processes.

§2. X-Ray Magnetic Scattering

The magnetic scattering amplitude has been reviewed by several authors.^{17, 18, 19)} We summarize here the expression of the amplitude in a form suitable to calculating the azimuthal angle dependence. The scattering geometry is shown in Fig. 3. Photon with frequency ω , momentum \mathbf{k}_i and polarization μ ($= \sigma$ or π) is scattered into the state with momentum \mathbf{k}_f and polarization μ' ($= \sigma'$ or π'). For the system with two magnetic sublattices A and B in the AF order, we write down the cross section for elastic scattering at magnetic Bragg peaks as

$$\left. \frac{d\sigma}{d\Omega'} \right|_{\mu \rightarrow \mu'} \propto \left| T_{\mu \rightarrow \mu'}^A(\mathbf{G}, \omega) - T_{\mu \rightarrow \mu'}^B(\mathbf{G}, \omega) \right|^2, \quad (2.1)$$

with

$$\begin{aligned} T_{\mu \rightarrow \mu'}^\eta(\mathbf{G}, \omega) = & -\frac{i\hbar\omega}{mc^2} \left(\frac{1}{2} \mathbf{L}^\eta(\mathbf{G}) \cdot \mathbf{A}'' + \mathbf{S}^\eta(\mathbf{G}) \cdot \mathbf{B} \right) \\ & + J_{\mu \rightarrow \mu'}^\eta(\mathbf{G}, \omega) + L_{\mu \rightarrow \mu'}^\eta(\mathbf{G}, \omega). \end{aligned} \quad (2.2)$$

where $\mathbf{G} = \mathbf{k}_f - \mathbf{k}_i$ is the scattering vector. The first term in eq. (2.2) represents a *non-resonant* term at sublattice η ($= A$ or B), with m and c being the electron mass and the velocity of photon, respectively.¹⁹⁾ $\mathbf{L}^\eta(\mathbf{G})$ and $\mathbf{S}^\eta(\mathbf{G})$ stand for the Fourier transform of the orbital and spin angular momentum density,²⁰⁾ and \mathbf{A}'' and \mathbf{B} are given by

$$\mathbf{A}'' = \mathbf{A}' - (\mathbf{A}' \cdot \hat{\mathbf{G}})\hat{\mathbf{G}}, \quad \mathbf{A}' = -4\sin^2\theta(\hat{\epsilon}' \times \hat{\epsilon}), \quad (2.3)$$

$$\mathbf{B} = \hat{\epsilon}' \times \hat{\epsilon} + (\hat{\mathbf{k}}_f \times \hat{\epsilon}')(\hat{\mathbf{k}}_f \cdot \hat{\epsilon}) - (\hat{\mathbf{k}}_i \times \hat{\epsilon})(\hat{\mathbf{k}}_i \cdot \hat{\epsilon}') - (\hat{\mathbf{k}}_f \times \hat{\epsilon}') \times (\hat{\mathbf{k}}_i \times \hat{\epsilon}), \quad (2.4)$$

where $\hat{\epsilon}$ and $\hat{\epsilon}'$ are the initial and scattered polarizations, and $\hat{\mathbf{k}}_i$, $\hat{\mathbf{k}}_f$, and $\hat{\mathbf{G}}$ are normalized vectors of \mathbf{k}_i , \mathbf{k}_f , and \mathbf{G} .

The second and third terms in eq. (2.2) represent the resonant contribution at the K edge, which originates from a second-order process that a photon is virtually absorbed by exciting the $1s$ electron to unoccupied states and then emitted by recombining the excited electron with the $1s$

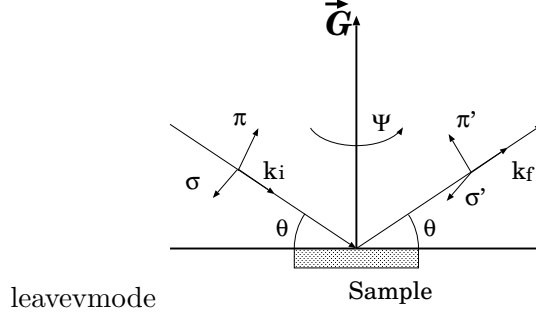


Fig. 3. Geometry of x ray scattering. Photon with polarization σ or π is scattered into the state of polarization σ' or π' at Bragg angle θ . The sample crystal is rotated by azimuthal angle ψ around the scattering vector $\mathbf{G} = \mathbf{k}_f - \mathbf{k}_i$.

core hole. The amplitude by the dipole process is expressed as

$$J_{\mu \rightarrow \mu'}^{\eta}(\mathbf{G}, \omega) = \sum_{\alpha \alpha'} (P'^{\mu'})_{\alpha}^{\dagger} M_{\alpha \alpha'}^{\eta}(\omega) P_{\alpha'}^{\mu}, \quad (2.5)$$

where the geometrical factors P^{μ} , $P'^{\mu'}$ are explicitly given in the Appendix, and the scattering tensor $M^{\eta}(\omega)$ is given by

$$M_{\alpha \alpha'}^{\eta}(\omega) = \sum_j \frac{m \omega_{jg}^2 \langle g | x_{\alpha} | j \rangle \langle j | x_{\alpha'} | g \rangle}{\hbar \omega - (E_j - E_g) + i\Gamma/2}. \quad (2.6)$$

Here x_{α} 's stand for the dipole operators, $x_1 = x$, $x_2 = y$, and $x_3 = z$ in the coordinate frame fixed to the crystal axes. The ground state $|g\rangle$ has an energy E_g , and the intermediate state $|j\rangle$, consisting of an excited electron on the $4p$ states and a hole on the $1s$ state, has an energy E_j ; $\omega_{jg} \equiv (E_j - E_g)/\hbar$. Quantity Γ is introduced to describe the life-time broadening due to the core hole. The amplitude by the quadrupole process is expressed as

$$L_{\mu \rightarrow \mu'}^{\eta}(\mathbf{G}, \omega) = \sum_{\gamma \gamma'} (Q'^{\mu'})_{\gamma}^{\dagger} N_{\gamma \gamma'}^{\eta}(\omega) Q_{\gamma'}^{\mu}, \quad (2.7)$$

where the geometrical factors, Q^{μ} , $Q'^{\mu'}$, are explicitly given in the Appendix, and the scattering tensor $N^{\eta}(\omega)$ is given by

$$N_{\gamma \gamma'}^{\eta}(\omega) = \frac{k^2}{12} \sum_{\ell} \frac{m \omega_{\ell g}^2 \langle g | z_{\gamma} | \ell \rangle \langle \ell | z_{\gamma'} | g \rangle}{\hbar \omega - (E_{\ell} - E_g) + i\Gamma/2}. \quad (2.8)$$

Here k is the wavenumber of the incident (and scattered) photon, and z_{μ} 's stand for the quadrupole operators, $z_1 = (\sqrt{3}/2)(x^2 - y^2)$, $z_2 = (1/2)(3z^2 - r^2)$, $z_3 = \sqrt{3}yz$, $z_4 = \sqrt{3}zx$, and $z_5 = \sqrt{3}xy$ in the coordinate frame fixed to the crystal axes. The intermediate state $|\ell\rangle$, consisting of an excited electron on the $3d$ states and a hole on the $1s$ states, has an energy E_{ℓ} ; $\omega_{\ell g} = (E_{\ell} - E_g)/\hbar$.

§3. 3d and 4p States at Co Sites

Each Co atom is in the $3d^7$ configuration under the cubic crystal field. We neglect small effects of the distortion such that $c/a < 1$. The ground state 4F of a free cobaltous ion is split into the representations Γ_4 and Γ_5 . Three degenerate states in the Γ_4 representation have lower energy than those in the Γ_5 representation. The spin of each ion is subjected to a strong exchange field and is oriented in its direction, forming an AF long range order. As mentioned before, we assume that the AF modulation direction \mathbf{Q} is one of the four body-diagonals in the fcc lattice.

As regards the orbitals, we introduce the pseudo-angular-momentum operator ℓ of magnitude 1 in the Γ_4 representation, such that the orbital-angular-momentum operator \mathbf{L} is given by $-(3/2)\ell$. Thereby, in the first approximation, the wave function of the state specified by $\ell_z = 0$ correspond to the configuration that $\varphi_0 \equiv d_{xy}$ is singly occupied (in other wards, d_{zx} and d_{yz} are doubly occupied); the state $\ell_z = \pm 1$ is such that $\varphi_{\pm 1} \equiv \mp \frac{1}{\sqrt{2}}(d_{zx} \pm id_{yz})$ is singly occupied. Connected with the spin through the spin-orbit coupling, ℓ becomes antiparallel to the spin direction. Thus the ground state gives the spin moment $\sim 3\mu_B$ and the orbital moment $\sim 1.5\mu_B$. As discussed by Kanamori,⁹⁾ quantum mechanical effects modify this classical ground state, making the magnetic moment close to the experimental value. Since we are aiming at analyzing qualitatively the RXMS intensity, we will not consider the quantum correction.

The unoccupied 3d states become occupied by an electron excited from the 1s state in the intermediate states of the quadrupole process. The scattering amplitudes of filling the unoccupied 3d states are usually cancelled out between those at the A and B sublattices. However, it is not the case for the unoccupied state in the Γ_4 representation, since this orbital is strongly coupled to the magnetic order through the spin-orbit coupling. We call this unoccupied state in the intermediate state as the $3d^*$ state with energy ϵ_d . This $3d^*$ state, which is represented as $\varphi'_{\mp 1}$ in the coordinate frame that the z axis is along the spin direction (the upper (lower) sign corresponds to the A (B) sublattice), is expressed in the coordinate frame fixed to the crystal axes as

$$\varphi'_{\mp 1} = D_{1\mp 1}^{(1)}(\alpha, \beta, \gamma)\varphi_1 + D_{0\mp 1}^{(1)}(\alpha, \beta, \gamma)\varphi_0 + D_{-1\mp 1}^{(1)}(\alpha, \beta, \gamma)\varphi_{-1}, \quad (3.1)$$

where $D_{mm'}^{(1)}(\alpha, \beta, \gamma)$ is the rotation matrix of the first rank,²¹⁾ with the Euler angles $\alpha = -3\pi/4$, $\beta = \arcsin \frac{1}{\sqrt{3}}$, $\gamma = 0$ for domain S_1 , $\alpha = \pi/2 + \arcsin 1/\sqrt{5}$, $\beta = \pi - \arcsin \sqrt{5/6}$, $\gamma = 0$ for domain S_2 , and $\alpha = -\arcsin 1/\sqrt{5}$, $\beta = \pi - \arcsin \sqrt{5/6}$, $\gamma = 0$ for domain S_3 . Substituting these states for $|\ell\rangle$ in eq. (2.8), we obtain the scattering tensor, which has an antisymmetric form,

$$N^A(\omega) - N^B(\omega) = \begin{pmatrix} 0 & 0 & 0 & 0 & 0 \\ 0 & 0 & 0 & 0 & 0 \\ 0 & 0 & 0 & d & f \\ 0 & 0 & -d & 0 & e \\ 0 & 0 & -f & -e & 0 \end{pmatrix}, \quad (3.2)$$

with d , e , and f being complex numbers.

The unoccupied $4p$ states at Co sites become occupied by an electron excited from the $1s$ state in the intermediate states of the dipole process. The scattering amplitudes of filling the $4p$ states are cancelled out between those at the A and B sublattices, unless the $4p$ states are coupled to the $3d$ states which constitute the magnetic order. One possible coupling is the intraatomic exchange interaction between the $4p$ and the $3d$ states. Since the occupied $3d$ states have finite orbital moment, this coupling makes the $4p$ levels split; at the A sublattice, the states $p'_1 = -\frac{1}{\sqrt{2}}(p'_x + ip'_y)$, $p'_0 = p'_z$ and $p'_{-1} = \frac{1}{\sqrt{2}}(p'_x - ip'_y)$ with down spin have energy $\epsilon_1, 0, \epsilon_2$; at the B sublattice, p'_1, p'_0, p'_{-1} with up spin have energy $\epsilon_2, 0, \epsilon_1$. Here $p'_{\pm 1}$ and p'_0 refer to the coordinate frame that the z axis is along the spin direction. The ϵ_1 and ϵ_2 are roughly evaluated as $\epsilon_1 = -0.056$ eV, $\epsilon_2 = -0.020$ eV.²²⁾ Another coupling is the mixing to the $3d$ states of neighboring Co atoms. What is effective to make the amplitude at the A sublattice different from at the B sublattice is the mixing to the $3d^*$ state.

To estimate the effects of these couplings, we use a cluster model that the $4p$ states at the central site are mixing to the $3d^*$ state of 12 neighboring Co atoms (Fig. 1). Thus the Hamiltonian matrix has 39×39 dimensions. The effect of the mixing to the $2p$ states of neighboring oxygens is implicitly included into the model by adjusting the energy of the $4p$ states. According to the experiment,³⁾ the main peak is at $\hbar\omega = 7.724$ keV and the pre-edge peak at $\hbar\omega = 7.707$ keV. Thereby we put $\epsilon_p - \epsilon_d = 17$ eV for the difference between the energy of the $4p$ states, ϵ_p , and that of the $3d^*$ states, ϵ_d , both at the central site. Note that both ϵ_p and ϵ_d are including the interaction energy with the $1s$ hole. The energy $\tilde{\epsilon}_d$ of the $3d^*$ state at the neighboring Co atoms is several eV's higher than that at the central site where the core hole exists, since the interaction with the $1s$ hole is not working there. We assume the difference to be $\tilde{\epsilon}_d - \epsilon_d = 4$ eV. Then we evaluate the off-diagonal part of the Hamiltonian matrix by using the Slater-Koster parameters, $(pd\sigma)$ and $(pd\pi)$,²³⁾ with the help of eq. (3.1). We assume $(pd\sigma) = -0.5$ eV together with an empirical relation $(pd\pi) = -(1/2)(pd\sigma)$.²⁴⁾ This size of the $(pd\sigma)$ value seems reasonable, since the $4p$ states are highly extended in space.

The Hamiltonian matrix can be numerically diagonalized. We find that three degenerate $4p$ states are split into the states with finite orbital moments. Substituting these eigenstates for the intermediate states in eq. (2.6), we calculate the scattering amplitude. As a reflection of the induced orbital moment for the $4p$ states, the scattering tensor has an antisymmetric form,

$$M^A(\omega) - M^B(\omega) = \begin{pmatrix} 0 & a & c \\ -a & 0 & b \\ -c & -b & 0 \end{pmatrix}, \quad (3.3)$$

with a , b , and c being complex numbers.

§4. Calculated Results in Comparison with Experiment

In the preceding section, we have studied the $3d$ and $4p$ states in the intermediate states of the RXMS. For calculating the scattering intensity, we have to estimate further several quantities. First, we evaluate the matrix elements for the dipole and quadrupole processes within the HF approximation.¹⁰⁾ They are given by

$$\langle 4p|r|1s \rangle \equiv \int_0^\infty R_{4p}(r)rR_{1s}(r)r^2dr = 1.52 \times 10^{-11} \text{ cm}, \quad (4.1)$$

$$\langle 3d|r^2|1s \rangle \equiv \int_0^\infty R_{3d}(r)r^2R_{1s}(r)r^2dr = 2.10 \times 10^{-20} \text{ cm}^2, \quad (4.2)$$

where $R_{1s}(r)$, $R_{4p}(r)$, and $R_{3d}(r)$ are radial wave functions for the $1s$, $4p$, and $3d$ states in the $3d^7$ configuration of a free cobaltous ion (see Fig. 2). Since the $1s$ state is well localized inside the ion radius, these values are to be good estimates in solids, with multiplying a factor 0.8. With these values and $k \sim 3.9 \times 10^8 \text{ cm}^{-1}$ around the K edge, we have $k^2|\langle 3d|r^2|1s \rangle|^2/(20|\langle 4p|r|1s \rangle|^2) \sim 1.5 \times 10^{-2}$, which is a measure of the ratio of the amplitude of the quadrupole process to that of the dipole process. Second, we assume that $|\mathbf{S}(\mathbf{G})| \sim 1.0$, $|\mathbf{L}(\mathbf{G})| \sim 0.8$, in the first term of eq. (2.3), for the scattering vectors $\mathbf{G} = (-\frac{1}{2}, -\frac{1}{2}, \frac{7}{2})$ and $(\frac{1}{2}, \frac{1}{2}, \frac{5}{2})$; these values are smaller than those for $\mathbf{G} = 0$, that is, the local orbital- and spin-angular momenta. This is consistent with the general tendency that $|\mathbf{S}(\mathbf{G})|$ and $|\mathbf{L}(\mathbf{G})|$ are decreasing with increasing values of \mathbf{G} .²⁵⁾ The precise values are not necessary for our qualitative analysis. Third, we use the experimental value 1.7 eV from the fluorescence measurement for the life-time broadening width Γ .²⁶⁾

Experimentally, Neubeck *et al.* have separated the contributions to the scattering intensity from each magnetic domain; the data are shown for $\mathbf{G} = (-\frac{1}{2}, \frac{1}{2}, \frac{7}{2})$ and $(\frac{1}{2}, -\frac{1}{2}, \frac{5}{2})$ in the K domain with $\mathbf{Q} = (\frac{1}{2}, -\frac{1}{2}, \frac{1}{2})$.³⁾ In this paper, we consider the K domain with $\mathbf{Q} = (\frac{1}{2}, \frac{1}{2}, \frac{1}{2})$, not identical to the experimental one. In our K domain, the scattering vectors $\mathbf{G} = (-\frac{1}{2}, -\frac{1}{2}, \frac{7}{2})$ and $(\frac{1}{2}, \frac{1}{2}, \frac{5}{2})$ correspond to the above experimental scattering vectors. Note that the $(1, -1, 0)$ crystal axis lies on the scattering plane at $\psi = 0$ in our definition of the geometrical factor (see the Appendix).

Figure 4 (a) shows the calculated intensity as a function of photon energy for $\mathbf{G} = (-\frac{1}{2}, -\frac{1}{2}, \frac{7}{2})$. The azimuthal angle is set to be $\psi = -46^\circ$, such that the $(1, 0, 0)$ crystal axis lies on the scattering plane. (This corresponds to the experimental geometry that the $(0, 1, 0)$ crystal axis lies on the scattering plane.) For the $\sigma \rightarrow \sigma'$ channel (lower panel), only one peak is found at the pre- K -edge position, in agreement with the experiment. This peak arises from the quadrupole process, since the dipole process is forbidden. The amplitude from the quadrupole process interferes with the non-resonant term, leading to an anti-resonant dip in the spectra. For the $\sigma \rightarrow \pi'$ channel (upper panel), a large peak is found at the main K -edge position in addition to the pre-edge peak, in good agreement with the experimental curve after correction for absorption.^{3, 27)} The intensity of the main peak depends on the S domains; for example, it is very small for domain S_3 .

Figure 4 (b) shows the calculated intensity as a function of photon energy for $\mathbf{G} = (\frac{1}{2}, \frac{1}{2}, \frac{5}{2})$. The

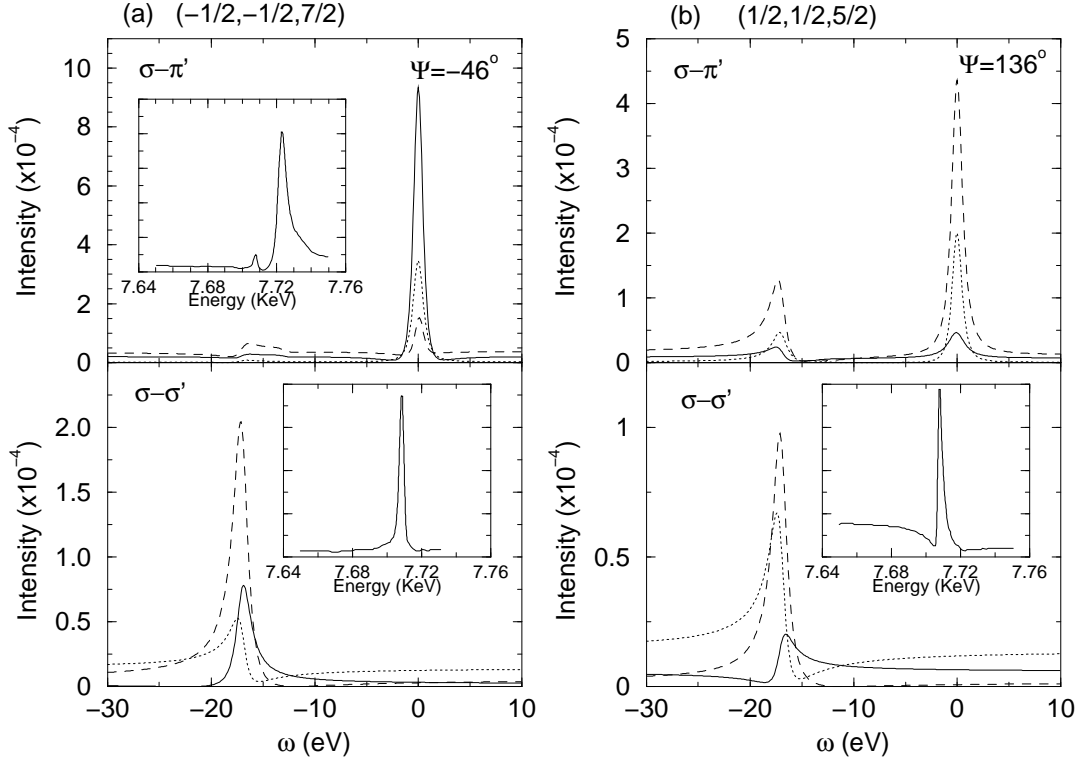


Fig. 4. Magnetic scattering intensity as a function of photon energy (a) for $\psi = -46^\circ$, $\mathbf{G} = (-\frac{1}{2}, -\frac{1}{2}, \frac{7}{2})$, and (b) for $\psi = 136^\circ$, $\mathbf{G} = (\frac{1}{2}, \frac{1}{2}, \frac{5}{2})$. The solid, dotted and broken lines represent the intensities from domains S_1 , S_2 , and S_3 in the same K domain with $\mathbf{Q} = (\frac{1}{2}, \frac{1}{2}, \frac{1}{2})$. The zero of energy is at the main peak. The upper and lower panels show the intensity for the $\sigma \rightarrow \pi'$ channel, and that for the $\sigma \rightarrow \sigma'$ channel, respectively. The insets show the experimental curves of ref. 3. The curve in the inset on the top panel in (a) is after absorption correction.

azimuthal angle is set to be $\psi = 136^\circ$, such that the $(1, 0, 0)$ crystal axis lies on the scattering plane. (This correspond to the experimental situation that the $(0, 1, 0)$ crystal axis lies on the scattering vector.) For the $\sigma \rightarrow \sigma'$ channel (lower panel), only the pre-edge peak is found, in agreement with the experiment. The anti-resonant dip is found below the pre-edge peak for domain S_1 . Such a dip is actually observed in the experiment (see the inset). For the $\sigma \rightarrow \pi'$ channel (upper panel), the main peak is found in addition to the pre-edge peak, but its intensity is much smaller than that for $\mathbf{G} = (-\frac{1}{2}, -\frac{1}{2}, \frac{7}{2})$. As already pointed out,³⁾ the intensity of the main peak is the smallest for domain S_1 . Experimentally, the main peak is not clearly seen. Combining this fact to the spectral shape of the pre-edge peak, we speculate that the experimental spectrum comes from domain S_1 .

Figure 5 shows the RXMS intensity for the $\sigma \rightarrow \pi'$ channel in the energy region of main peak, which is calculated with neglecting the intraatomic exchange interaction between the $4p$ and $3d$

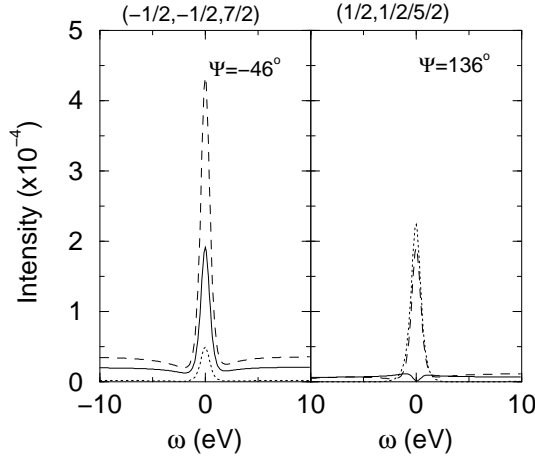


Fig. 5. Magnetic scattering intensity for the $\sigma \rightarrow \pi'$ channel in the energy region of main peak, calculated with neglecting the intraatomic exchange interaction between the $4p$ and $3d$ states. The solid, dotted and broken lines represent the intensities from domains S_1 , S_2 and S_3 .

states. The intensities are nearly half of those shown in Fig. 4, indicating that the contribution of the intraatomic exchange interaction is comparable to that of the p - d mixing to the $3d$ states of neighboring Co atoms. Note that the latter contribution increases according to roughly the square of the strength of the p - d mixing. It is highly probable that the effect of the intraatomic exchange interaction is suppressed by a band formation of the $4p$ states, since the energy splittings caused by the exchange interaction are averaged out at the A and B sublattices in the states with small momenta. For making clear this point, however, it is necessary to perform a band calculation, which has not been completed.

Figure 6 shows the calculated intensity as a function of the azimuthal angle for $\mathbf{G} = (-\frac{1}{2}, -\frac{1}{2}, \frac{7}{2})$ and $(\frac{1}{2}, \frac{1}{2}, \frac{5}{2})$. We find rather complicated behavior; for example, for the $\sigma \rightarrow \pi'$ channel at $\mathbf{G} = (\frac{1}{2}, \frac{1}{2}, \frac{5}{2})$, the main peak grows considerably while the pre-edge peak shrinks, with increasing values of ψ . One reason for such complicated behavior is that the scattering vector is not along the crystal axes. The experimental data are not available to make comparison.

§5. Concluding Remarks

We have analyzed the recent experiment for the RXMS intensity for CoO using a cluster model. The spins and orbitals are ordered with the same wavevector under strong spin-orbit coupling. The point different from the case of ordinary orbital order is that the scattering tensor becomes antisymmetric. The cluster calculation gives a reasonable description for the RXMS intensity. We

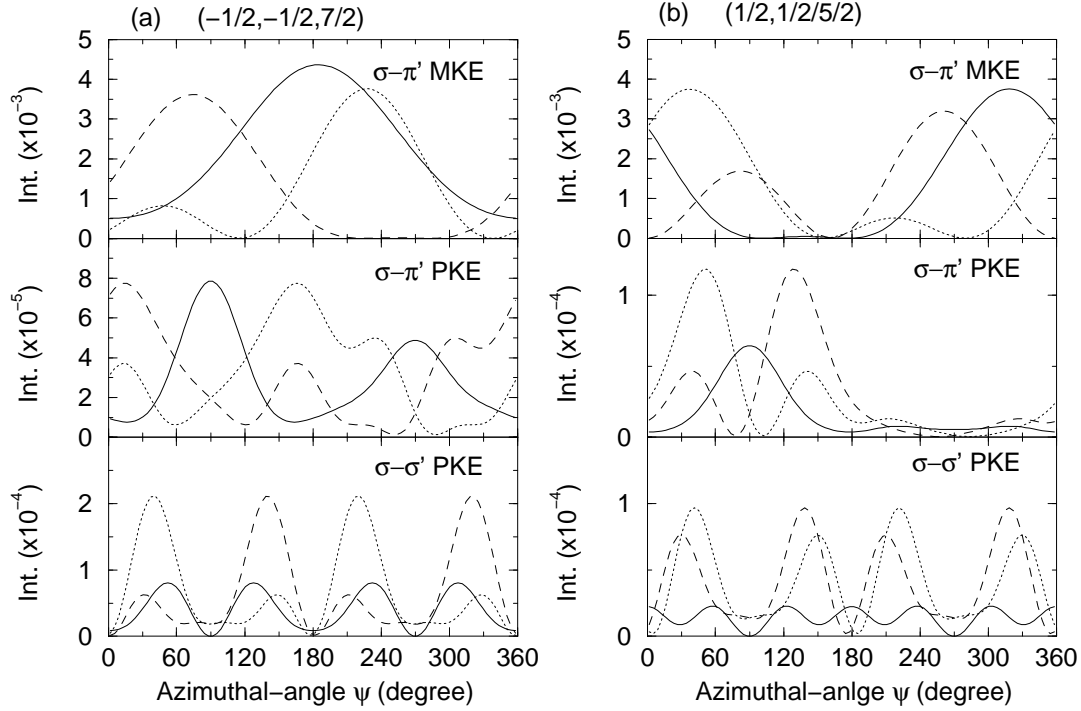


Fig. 6. Magnetic scattering intensity as a function of azimuthal angle ψ ; (a) for $\mathbf{G} = (-\frac{1}{2}, -\frac{1}{2}, \frac{7}{2})$, and (b) for $\mathbf{G} = (\frac{1}{2}, \frac{1}{2}, \frac{5}{2})$. The upper panel is for the main K -edge (MKE) peak, and the middle and lower panels are for the pre K -edge (PKE) peak. The solid, dotted and broken lines represent the intensities from domains S_1 , S_2 and S_3 .

have found that the $4p$ states of Co are modified not only by the intraatomic exchange coupling to the $3d$ states but also by the orbital moment of the $3d$ states of neighboring Co atoms through the p - d mixing. Thereby the orbital moment is induced in the $4p$ states, and a considerable intensity is brought about through the dipole process. The p - d mixing mechanism reminds us of the magnetic circular dichroism (MCD) for the K -edge absorption in the ferromagnetic metals Fe, Co, and Ni,²⁸⁾ where the MCD intensity comes mainly from the orbital moment induced in the $4p$ states through the mixing to the $3d$ states of neighboring Co atoms.^{29,30)}

We have also found the pre-edge peak in the RXMS intensity. It originates from the quadrupole process. This contrasts with the pre-edge peak in the resonant scattering for the orbital order in LaMnO_3 , which is predicted to be generated by the dipole process.¹⁶⁾ We have also calculated the azimuthal angle dependence of the RXMS intensity, which shows rather complicated behavior. We are waiting for future experiments to make comparison.

In this paper, we have used a simple cluster model for analyzing qualitatively the experimental data. Since the $4p$ states are considerably extended in space, it is much better to treat them as a

band. We speculate that the effect of the intraatomic exchange interaction is suppressed by a band formation of the $4p$ states. A study based on the band calculation is now under progress.

Acknowledgment

We would like to thank W. Neubeck for kindly informing the experimental values for the ω , χ , and ϕ angles in a 4-circle diffractometer. We also acknowledge T. Jo and J. Mizuki for valuable discussions. This work was partially supported by a Grant-in-Aid for Scientific Research in Priority Area, “Novel Quantum Phenomena in Transition Metal Oxides -Spin·Charge·Orbital Coupled Systems-” No. 407, from the Ministry of Education, Science, Sports and Culture.

Appendix: Geometrical Factors

We outline the derivation of the geometrical factors in the coordinate frame fixed to the crystal axes and summarize the result here.

A.1 Dipole Transition

In the coordinate frame (x', y', z') that the z' axis is the propagation direction of photon, the dipole operators for *circular* polarization are given by

$$\frac{1}{\sqrt{2}}(x' \pm iy') = \mp \left(\frac{4\pi}{3}\right)^{1/2} Y_{1\pm 1}(\theta', \varphi') r', \quad (\text{A}\cdot 1)$$

where r' , θ' , φ' are corresponding polar coordinates. We represent these operators in the coordinate frame (x'', y'', z'') that the z'' axis is along the scattering vector \mathbf{G} and y'' axis is contained in the scattering plane (Fig. 3). This is done by the relation,²¹⁾

$$Y_{\ell m'}(\theta', \varphi') = \sum_m D_{mm'}^{(\ell)}(\alpha, \beta, \gamma) Y_{\ell m}(\theta'', \varphi''), \quad (\text{A}\cdot 2)$$

where $\ell = 1$, $m' = \pm 1$ with the Euler angles α, β, γ being $\alpha = \pi/2$, $\beta = \pi/2 + \theta$, and $\gamma = -\pi/2$ for incident photons, and being $\alpha = \pi/2$, $\beta = \pi/2 - \theta$, and $\gamma = -\pi/2$ for scattered photons. According to the rotation of the crystal by azimuthal angle ψ around the scattering vector \mathbf{G} , we replace

$$Y_{1m}(\theta'', \varphi'') \longrightarrow Y_{1m}(\theta'', \varphi'') e^{im\psi''}. \quad (\text{A}\cdot 3)$$

Next we then express $Y_{1m}(\theta'', \varphi'')$'s in the coordinate frame (x''', y''', z''') fixed to the crystal axes with the help of eq. (A·2), with $\alpha = -3\pi/4$, $\beta = \arcsin \sqrt{2/51}$, $\gamma = 0$, for $\mathbf{G} = (-\frac{1}{2}, -\frac{1}{2}, \frac{7}{2})$, and with $\alpha = \pi/4$, $\beta = \arcsin \sqrt{2/27}$, $\gamma = 0$, for $\mathbf{G} = (\frac{1}{2}, \frac{1}{2}, \frac{5}{2})$. Finally we change the expressions in the circularly polarized base into those in the linearly polarized base. Thus we obtain the geometrical factor for incident photon P^μ ($\mu = \sigma$ or π) as

$$\begin{aligned} (P^\sigma)_1 &= \pm(\cos \beta \cos \psi + \sin \psi)/\sqrt{2}, \\ (P^\sigma)_2 &= \pm(\cos \beta \cos \psi - \sin \psi)/\sqrt{2}, \end{aligned}$$

$$(P^\sigma)_3 = -\sin \beta \cos \psi, \quad (\text{A}\cdot 4)$$

$$\begin{aligned} (P^\pi)_1 &= \pm [\sin \theta (\cos \beta \sin \psi - \cos \psi) + \cos \theta \sin \beta] / \sqrt{2}, \\ (P^\pi)_2 &= \pm [\sin \theta (\cos \beta \sin \psi + \cos \psi) + \cos \theta \sin \beta] / \sqrt{2}, \\ (P^\pi)_3 &= (-\sin \theta \sin \beta \sin \psi + \cos \theta \cos \beta). \end{aligned} \quad (\text{A}\cdot 5)$$

The upper and lower signs in eqs. (A·4) and (A·5) correspond to $\mathbf{G} = (-\frac{1}{2}, -\frac{1}{2}, \frac{7}{2})$ and $(\frac{1}{2}, \frac{1}{2}, \frac{5}{2})$, respectively. We also obtain the geometrical factor for scattered photon $P^{\mu'}$ ($\mu' = \sigma'$ or π') from eqs. (A·4) and (A·5) with replacing $\sin \theta$ by $-\sin \theta$. Note that the scattering plane for $\psi = 0$ contains the $(1, -1, 0)$ crystal axis in this definition of the coordinate frame.

A.2 Quadrupole Transition

In the coordinate frame (x', y', z') that the z' axis is the propagation direction of photon, the quadrupole operators for *circular* polarization are given by

$$\frac{1}{2} \frac{1}{\sqrt{2}} z' (x' \pm iy') = \mp \left(\frac{\pi}{15} \right)^{1/2} Y_{2\pm 1}(\theta', \varphi'). \quad (\text{A}\cdot 6)$$

We represent these operators in the coordinate frame fixed to the crystal axes by following the same procedure as for the dipole transition. We change the expressions in the circularly polarized base into those in the linearly polarized base. Thus we obtain the geometrical factor for incident photon Q^μ ($\mu = \sigma$ or π) as

$$\begin{aligned} (Q^\sigma)_1 &= -\cos \theta \cos \beta \cos 2\psi - \sin \theta \sin \beta \sin \psi, \\ (Q^\sigma)_2 &= (\sqrt{3}/2) \cos \theta \sin^2 \beta \sin 2\psi + (\sqrt{3}/2) \sin \theta \sin 2\beta \cos \psi, \\ (Q^\sigma)_3 &= \mp \cos \theta \sin \beta (\cos \beta \sin 2\psi + \cos 2\psi) / \sqrt{2} \\ &\quad \mp \sin \theta (\cos 2\beta \cos \psi - \cos \beta \sin \psi) / \sqrt{2}, \\ (Q^\sigma)_4 &= \mp \cos \theta \sin \beta (\cos \beta \sin 2\psi - \cos 2\psi) / \sqrt{2} \\ &\quad \mp \sin \theta (\cos 2\beta \cos \psi + \cos \beta \sin \psi) / \sqrt{2}, \\ (Q^\sigma)_5 &= \cos \theta [1 - (1/2) \sin^2 \beta] \sin 2\psi - (1/2) \sin \theta \sin 2\beta \cos \psi, \\ (Q^\pi)_1 &= -(1/2) \sin 2\theta \cos \beta \sin 2\psi - \cos 2\theta \sin \beta \cos \psi, \\ (Q^\pi)_2 &= -(\sqrt{3}/4) \sin 2\theta \sin^2 \beta \cos 2\psi - (\sqrt{3}/2) \cos 2\theta \sin 2\beta \sin \psi \\ &\quad - (\sqrt{3}/2) \sin 2\theta [1 - (3/2) \sin^2 \beta], \\ (Q^\pi)_3 &= \pm (1/2\sqrt{2}) \sin 2\theta \sin \beta (\cos \beta \cos 2\psi - \sin 2\psi) \\ &\quad \pm \cos 2\theta (\cos 2\beta \sin \psi + \cos \beta \cos \psi) / \sqrt{2} \\ &\quad \mp (3/4\sqrt{2}) \sin 2\theta \sin 2\beta, \\ (Q^\pi)_4 &= \pm (1/2\sqrt{2}) \sin 2\theta \sin \beta (\cos \beta \cos 2\psi + \sin 2\psi) \\ &\quad \pm \cos 2\theta (\cos 2\beta \sin \psi - \cos \beta \cos \psi) / \sqrt{2} \end{aligned} \quad (\text{A}\cdot 7)$$

$$\begin{aligned}
& \mp (3/4\sqrt{2}) \sin 2\theta \sin 2\beta, \\
(Q^\pi)_5 &= -(1/2) \sin 2\theta [1 - (1/2) \sin^2 \beta] \cos 2\psi \\
&+ (1/2) \cos 2\theta \sin 2\beta \sin \psi - (3/4) \sin 2\theta \sin^2 \beta,
\end{aligned} \tag{A-8}$$

where $\beta = \arcsin \sqrt{2/51}$ for $\mathbf{G} = (-\frac{1}{2}, -\frac{1}{2}, \frac{7}{2})$, and $\beta = \arcsin \sqrt{2/27}$ for $\mathbf{G} = (\frac{1}{2}, \frac{1}{2}, \frac{5}{2})$. The upper and lower signs in eqs. (A-7) and (A-8) correspond to $\mathbf{G} = (-\frac{1}{2}, -\frac{1}{2}, \frac{7}{2})$ and $(\frac{1}{2}, \frac{1}{2}, \frac{5}{2})$. We also obtain the geometrical factor for scattered photon $Q'^{\mu'}$ ($\mu' = \sigma'$ or π') from eqs. (A-7) and (A-8) with replacing $\sin \theta$ and $\sin 2\theta$ by $-\sin \theta$ and $-\sin 2\theta$, respectively.

-
- [1] K. Namikawa, M. Ando, T. Nakajima and H. Kawata: J. Phys. Soc. Jpn. **54** (1985) 4099.
 - [2] J. P. Hill, C.-C. Kao and D. F. McMorrow: Phys. Rev. B **55** (1997) R8662.
 - [3] W. Neubeck, C. Vettier, K.-B. Lee and F. de Bergevin: Phys. Rev. B **60** (1999) R9912.
 - [4] A. Stunault, F. de Bergevin, D. Wermeille, C. Vettier, Th. Brückel, N. Bernhoeft, G. J. McIntyre, and J. Y. Henry: Phys. Rev. B **60** (1999) 10170.
 - [5] C. G. Shull, W. A. Strauser and E. Q. Wollan: Phys. Rev. **83** (1951) 333.
 - [6] More precisely, the angle between the modulation vector and the spin direction is a little smaller than 90° . See, D. Herrmann-Ronzaud, P. Burlet and J. Rossat-Mignod: J. Phys. C **11** (1978) 2123. We disregard this deviation in the calculation.
 - [7] B. van Laar: Phys. Rev. **138** (1963) A581.
 - [8] T. Shishido and T. Jo: J. Phys. Soc. Jpn. **67** (1998) 2637.
 - [9] J. Kanamori: Prog. Theor. Phys. **17** (1957) 177.
 - [10] R. Cowan: *The Theory of Atomic Structure and Spectra* (University of California Press, Berkeley, 1981).
 - [11] Y. Murakami, J. P. Hill, D. Gibbs, M. Blume, I. Koyama, M. Tanaka, H. Kawata, T. Arima, Y. Tokura, K. Hirota and Y. Endoh: Phys. Rev. Lett. **81** (1998) 582.
 - [12] S. Ishihara and S. Maekawa: Phys. Rev. Lett. **80** (1998) 3799; Phys. Rev. B **58** (1998) 13449.
 - [13] I. S. Elfimov, V. I. Anisimov and G. Sawatzky: Phys. Rev. Lett. **82** (1999) 4264.
 - [14] M. Benfatto, Y. Joly and C. R. Natori: Phys. Rev. Lett. **83** (1999) 636.
 - [15] M. Takahashi, J. Igarashi and P. Fulde: J. Phys. Soc. Jpn. **68** (1999) 2530.
 - [16] M. Takahashi, J. Igarashi and P. Fulde: J. Phys. Soc. Jpn. **69** (2000) 1614.
 - [17] F. de Bergevin and M. Brunel: Acta Crystallogr., Sect. A: Cryst. Phys., Diff., Theor. Gen. Crystallogr. **37** (1981) 324.
 - [18] M. Blume: J. Appl. Phys. **57** (1985) 3615.
 - [19] M. Blume and D. Gibbs: Phys. Rev. B **37** (1988) 1779.
 - [20] In general, $\mathbf{L}(\mathbf{G})$ is similar to the Fourier transform of the orbital angular momentum density, but is not exactly reduced to that, except for $\mathbf{G} = 0$. See ref. 19 for the explicit form.
 - [21] M. E. Rose: *Elementary Theory of Angular Momentum*, (John Wiley & Sons Inc., New York, 1957).
 - [22] Setting the energy of the state p'_0 as the origin, we estimate $\epsilon_1 = -\frac{3}{15}G^1 + \frac{6}{245}G^3$, $\epsilon_2 = -\frac{15}{245}G^3$, with G^1 and G^3 being the Slater integrals between the $4p$ and $3d$ states. We evaluate G^1 and G^2 within the ion radius as $G^1 \sim G^3 = 0.4$ eV, since the $4p$ states lose their meaning outside the ion radius, and further multiply a factor 0.8 to those values to take account of solid-state effect.
 - [23] J. C. Slater and G. F. Koster: Phys. Rev. **94** (1954) 1498.
 - [24] L. F. Mattheiss: Phys. Rev. B **5** (1972) 290.

- [25] V. Fernandez, C. Vettier, F. de Bergevin, C. Giles, and W. Neubeck: Phys. Rev. B **57** (1998) 7870.
- [26] F. de Bergevin, M. Brunel, R. M. Galéra, C. Vettier, D. Wermeille, N. Bernhoeft, S. Langridge, C. Dufour, and G. Marchat: Phys. Rev. B **46** (1992) 10772.
- [27] As shown in ref. 3, the absorption correction makes the intensity of the main peak enhanced 5 \sim 10 times larger than that of the pre-edge peak. For the details of absorption corrections, see also K. Dumesnil, A. Stunault, Ph. Mangin, C. Vettier, D. Wermeille, N. Bernhoeft, S. Langridge, C. Dufour, and G. Marchal: Phys. Rev. B **58** (1998) 3172.
- [28] G. Schütz, W. Wagner, W. Wilhelm, P. Kienle, R. Zeller, R. Frahn, and G. Materlik: Phys. Rev. Lett. **58** (1987) 737.
- [29] J. Igarashi and K. Hirai: Phys. Rev. B **50** (1994) 17820.
- [30] J. Igarashi and K. Hirai: Phys. Rev. B **53** (1996) 6442.